Modeling of heat leak effect in round trip efficiency for Brayton pumped heat energy storage with liquid media, by cooling and heating of the reservoirs tanks.

D. Salomone-González, P. L.Curto-Risso, F. Favre

Facultad de Ingeniería, Universidad de la República, Montevideo, Uruguay

Abstract

For a pumped heat energy storage technology with commercial solar salt and a cold fluid such as methanol, the performance in long times of the Brayton like model associated to the losses of the four tanks (two high temperature units and two low temperature units) was studied. A round trip efficiency evaluation model linked with the heat leak coefficient was proposed for the sensible storage tanks, considering the losses for each face exposed to the environment. The different energy leaks and temperatures in the tanks were calculated for hourly climatic fluctuations during a reference year for a reference city. A zero-dimensional model was developed where radiation (direct and diffuse), convection and conduction effects were considered. The obtained results showed that for long periods, time and insulation thickness have a significant influence on the performance of the technology for long periods. For Brayton pumped heat energy storage technology with solar salts the round trip efficiency, which can be reduced daile by 0.4% even for a considerable insulation thickness of around 10% of the tank diameter. Winter-summer climatic conditions do not show a significant difference for tanks at higher temperatures, but as the temperature decreases, the effect becomes more visible but not decisive for the performance of the technology. The relatively high crystallization point of solar salt represents a significant solidification risk that limits the operation of the PHES technology during waiting periods for a surplus power to charge the system.

Keywords: Energy storage, Molten salts, Coupled Brayton model, Round trip efficiency, Heat leak model.

1. Introduction

Among some of the latest energy storage technologies under development, the thermal type system called pumped heat energy storage (PHES) is one of the most promising since, given its high theoretical efficiency and operational characteristics, it has several advantages over other alternatives such as chemical batteries or the already known mechanical systems PHS (pumped hydro storage) or CAES (compressed air energy storage). Its extended life cycle reaches a useful life of approximately 30 years, requires low maintenance and is not limited by geographic formations since its installation does not depend on the previous existence of natural formations. In fact, the total space used by a PHES system is one of the smallest among storage technologies because of its high energy density [1]. In addition, it does not depend on fossil fuels, therefore, it does not produce any type of environmental pollution and the technology uses materials that are fully available, economical and not toxic to the environment as is the case with many of the components of chemical batteries. On the downside, the technology is still under development, so the purchase of some of its specific components may be limited by increased investment costs. High temperatures are also a constraint when choosing compressors, since there is no massive commercial development of equipment that can tolerate such high values, which will substantially increase costs. Another disadvantage associated with temperatures is that storage systems cannot supply energy indefinitely and the duration of this supply is limited by the long-term storage capacity. It is at this point that this article is about understanding how storage losses influence the performance of the technology over time [1].

The use of PHES technology is based on energy utilization in times of surplus production or cheap electricity prices to generate thermal energy through a heat pump cycle (system load), since thermal energy can be stored in tanks at a relatively low cost. If electricity demand increases, the stored thermal energy can be used to generate electrical energy through a power generation cycle (system discharge) such as the Joule-Brayton [2].

Energy storage in sensible heat reservoirs is the simplest and most economical thermal method against the new trends such as latent or thermochemical storage. Sensible energy can be stored in both solid and liquid media. There is a lot of experience in the study of packed bed systems and only a few authors have focused on liquid media. Although there are no commercial PHES systems currently installed, pilot tests have been evaluated and mathematical models have been formulated that refer to higher efficiency and lower cost of rock reservoirs [3, 4]. However, as it seeks to understand the long-term behavior of PHES, the lower performance of liquid media systems is offset by their higher storage potential over time. Rapid stratification loss is one of the major shortcomings of packed bed and suggests that energy storage in liquid media is more beneficial for longer-term operations [5]. For this reason, this paper chooses to describe the main characteristics of four-tanks PHES storage systems with commercial solar salt and methanol.

The generic scheme of the proposed system operation is

Nomenclature

A	area (m^2)	*Greek letters*	
a_s	absorptivity of different materials	α	internal irreversibility
b	direct ratio	β	external irreversibility
c_p	specific heat (J/kgK)	γ	adiabatic coefficient
C	calorific capacity (J/K)	Γ	heat capacity ratio
d	thermal diffusivity (m^2/s)	δ	inclination angle (rad)
D	diameter (m)	ϵ_i	efficiencies
e	tickness (m)	ε	emissivity
E_b	blackbody emissive power (W/m^2)	η	heat engine efficiency
f_d	diffuse fraction	θ_z	zenital angle (rad)
F_{ij}	radiation shape factors	θ	irradiation angle (rad)
g	acceleration due to gravity	κ_T	clarity index
G_{bi}	direct radiation (W/m^2)	μ	viscosity (kg/ms)
G_{dic}	circumsolar diffuse radiation (W/m^2)	ν	COP-coefficient of performance
G_{dii}	isotropic diffuse radiation (W/m^2)	ρ	density (kg/m^3)
G_i	incident irradiation ((W/m^2)	ρ_g	ground solar reflectance
G_{ri}	reflexed irradiation (W/m^2)	ξ	heat leak coefficient
Gr	Grashof number		
h	heat transfer coefficient (W/m^2K)	*Subscript*	
H	height (m)	a	air wall
i_e	isobaric expansion coefficient	c	compressor
J	radiosity (W/m^2)	C	convection
k	conductivity (W/mK)	f	floor
L	characteristic length (m)	g	ground
M	mass (kg)	G	solar radiation
$\dot{m}$	mass flow (kg/s)	HE	heat engine cycle
Nu	Nusselt number	HP	heat pump cycle
P	pressure (MPa)	H	high pressure zone
Pr	Prandtl number	i	inside
Q	heat (W)	K	conduction
r	pressure ratio (turbine or compressor)	L	low pressure zone
Re	Reynolds number	ℓ	liquid
s	natural-forced factor	n	net
S_t	Stanton number	r	roof
S	shape factor for ground (m)	R	radiation
t	time (s)	s	storage
T	temperature (K)	sky	sky
T_b	atmospheric transmittance	t	turbine
w	wind speed (m/s)	w	waiting
Y	dimensionless factor HE	0	ambient
z	salt level (m)	1-4	cycle points
Z	dimensionless factor HP		

shown in Fig. 1, where the directions of the working fluid flow (usually Argon or air) can be seen, either during charge (light blue) or discharge (dark blue). It is also shown the different processes and their equipment involved (compression, expansion and storage in four tanks at low temperature with cold fluids and at high temperature with solar salts). A more detailed description of the cycles is presented in Salomone et al. [2].

As shown in Fig. 1 the thermodynamic model presented in Salomone et al. [2] incorporates the internal irreversibilities from non-isentropic expansion and compression processes in the turbine (expander) and compressor (accounted for as isentropic efficiencies ϵ_t and ϵ_c respectively) and the pressure drop on the high and low temperature sides (expressed as percent pressure drop, $\Delta P/P_0$, where P_0 is the initial value). On the other hand, the external irreversibilities take into account the parameters for the coupling of the working fluid to the external

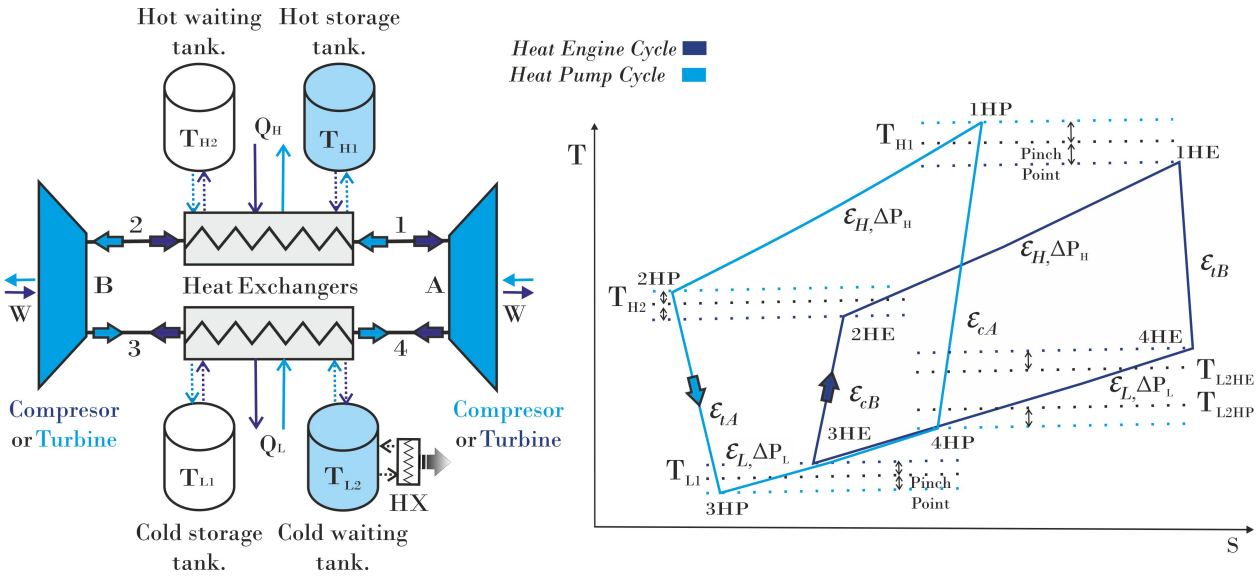

Figure 1: T-S diagram of the charge HP and discharge HE cycle and scheme of the corresponding components.

liquid medium in the high and low reservoirs (ϵ_H and ϵ_L respectively). The heat leak coefficient in this article is evaluated separately. For simplicity, the parameters α and β, for internal and external irreversibilities respectively, are defined such that [6]:

$$\epsilon_{c,t} = 1 - \alpha \tag{1}$$

$$\Delta P_i / P_0 = 1 - (1 - \alpha/5)^{\frac{\gamma}{\gamma-1}} \tag{2}$$

$$\epsilon_{H,L} = 1 - \beta \tag{3}$$

Where γ is the adiabatic coefficient of the working fluid.

To stabilize the system and extract the heat generated by the irreversibilities, an external heat exchanger (HX) is usually installed or, if the time is enough, the tank is left exposed to ambient temperature until the next charging period. This energy extracted from the system can be used for other services such as air conditioning or water heating. For this reason the tank at T_{L2} usually does not require insulation [2].

In short, when there are electrical surpluses, the system is charged in heat pump (HP) mode for a time (charging time) usually limited by the capacity of the reservoirs. The energy is stored until the demand requires it (storage time) and discharged with the heat engine (HE) mode until the hot tank is empty (discharging time). Then, it waits until a new power surplus occurs (waiting time) while the conditions are stabilized (removing the heat produced by the irreversibilities) to restart the cycle in heat pump mode. A chronological scheme of this operation is presented in Fig. 2.

Considering the simplicity of the technology, it is necessary to dedicate a special section to the behavior of the liquid energy storage (both for molten salts and cold fluids), since it is an important component of PHES systems. For this reason it is particularly interesting to evaluate its behavior, especially if seasonal storage is needed (a storage time that may require several days or even weeks of storage).

Although there is experience with molten salt reservoirs to solar plants [7, 8] there are only a few studies referring to liquid type PHES and no literature was found referring specifically to the cooling process of molten salt tanks and the heating of cold fluids for PHES over time and, especially, of some key aspects such as the effects in the round trip efficiency or the risk of crystallization.

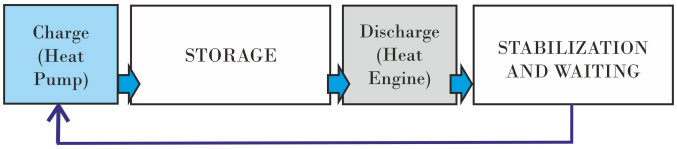

Figure 2: Scheme of cronological steps for PHES.

The first PHES proposals involving operation through a Joule-Brayton cycle were studied by Desrues and Ruer. [9]. The technology uses Argon as working fluid and refractory material in the high and low pressure tanks. Storage temperatures were as high as 1273K and good theoretical efficiencies of about 65% were obtained. Later, White and Mc.Tigue et al. [5] analyzed the configuration proposed by Desrues for various materials to develop correlations for estimating losses and conducted studies on the behavior of temperature variations across packed beds. In solid reservoirs, tank losses can reduce the efficiency proposed by Desrues by 10-15%. Guo et al. [10] developed a finite-time numerical model to estimate the system performance, obtaining values in the order of 20-40% global efficiency. Another researcher who became interested in Brayton-type PHES was Howes [11] which focused on the Ericcson-type reversible heat engine model (later Joule-Brayton) in combination with thermal energy storage using gravel, Argon as operating fluid and alternative devices instead of turbomachines. The most important achievement was the construction of a first prototype of solid storage PHES. The main PHES studies were done on solid storage, but in order to increase efficiencies, lower the cost of storage tanks and operate at low pressures, high temperature fluids appeared as storage media for the heat treatment

industry and in concentrated solar power plants (solar towers) [12]. The technology is similar to the previous since that tanks with liquid and heat exchangers are used to store energy. In the same line as White, Farres et al. [3] studied on solar salts and thermal oils for high-temperature reservoirs and cold fluids for low-temperature reservoirs, adding intermediate heating to achieve efficiencies greater than 50%. Also Laughlin [4] calculated the round-trip efficiency as a function of the polytropic efficiency and presented design equations for the heat exchangers as well as a complete economic balance based on the prices of the equipment and the different fluids involved in the system. He also compared Argon and Nitrogen as working fluids with a thorough analysis of the characteristics of the fluids involved. Molten salts and their properties have been studied by several authors such as Turchi [12] or Ferri [13], among others for use in solar plants. Given the high profitability of these systems, ways have been sought to optimize the technology and, particularly, to improve the insulation of the tanks for long-term storage.

Although many papers related to the process of heat transfer to the environment from hot or cold tanks can be found in the literature, to the best of the authors knowledge there are no studies that investigates the cooling process of molten salt tanks and the heating of cold fluids as a whole specifically associated with PHES technology. Schulte-Fischedick carried out an analysis of molten salt thermal storage system cooling to deepen the understanding of the energy wasted to the environment and the velocity and temperature distribution. Zaversky et al. [7] developed a transient model of a solar salt storage tank and simulated it over time for an existing solar thermal power plant. Wan et al. [14] proposed a coupled thermal performance evaluation model to evaluate the heat losses and temperature distributions of the tank and then adopted the finite element method to investigate the mechanical performance of the tank under different working conditions and Araujo et al. [8] presented a mathematical model to evaluate the heat losses of a sensible heat storage tank for a concentrated solar power plant.

The novelty of this work is the study of combined heat leak effect of high and low temperature storage technology on round trip efficiency, RTE (this allows to analyze the long-time effects). In short, this model analyzes the joint behavior for the four tanks of the PHES technology and its effect on RTE, for different storage times.

2. Energy storage system description.

2.1. Storage Reservoirs

A scheme of the storage tanks, the global thermal losses and the influencing factors is presented in the Fig. 3. Sensible heat reservoirs generally have a cylindrical geometry and are vertical. At low pressure, the liquid occupies a large part of the tank and a fraction remains with air above the liquid surface. The volume of air rises as the liquid is discharged and falls as it is charged (a vent valve is added to avoid overpressure problems and to avoid crystallization of the liquids; electrical heaters can be included at the bottom of the tanks.). In the hot tank heat leak (Q_i) comes from the roof (Q_r) and lateral walls in contact with the liquid and interior air (Q_ℓ and Q_a), under the influence of environmental factors such as ambient temperature (ground or air), sky temperature, wind speed and incident solar radiation. As for the loss through the floors (Q_f), it is worth mentioning that the tank foundations must be thought both in order to support the weight of the material and the contained liquid and to minimize thermal losses, however, there is experience in reservoir design for concentrating solar power plants with specific purposes of reducing this leakage. Many use layers of foam glass and refractory bricks (or even bricks with air ducts) [14].

One of the most important steps in the design process of liquid storage systems for PHES is the correct selection of the materials based on their properties. In particular, the thermal conductivity of the insulation is the primary factor in eliminating heat loss. The most common insulators can be mineral wool, glass wool, foams, microporous materials and ceramic fibers. For cold reservoirs can be polyurethane foam, expanded polystyrene, expanded perlite, among others. In addition to the increased costs associated with reduced performance due to heat leak, the absence or bad condition of insulation, especially in tanks containing high temperature products, could lead to material losses, fires, harmful environmental impact or even harm to people.

The properties of some of the different materials that usually appear in the configuration of solar salt and cold fluid tanks are shown in Table 1. It is noted that the thermal conductivity depends on the operating temperature. To complete the design of the exposed storage tank wall, it is assumed that the insulation layer is followed by a sheet metal protection (e.g. zinc, aluminum or galvanized steel). This external protective layer has a contribution to the thermal conductivity that can be considered negligible, however, its optical properties contribute to the radiative heat transfer to the outside [7].

Table 1: Parameters of heat storage and cold fluid tank materials for this article (T in K).

Material	Density (kg/m^3)	Conductivity (W/mK)
Steel Wall	7830	22.02 [14]
Mineral Wool	350	$8.67{\cdot}10^{-3} + 2.15{\cdot}10^{-4}T$ [14]
Refractory firebrick	800	$0.61 + 5.8{\cdot}10^{-4}T$ [14]
Foamglass	115	$4.3{\cdot}10^{-2} + 1.3{\cdot}10^{-4}T$ [14]
Polyurethane foam	35	0.0199 – 0.0278 [15]
Semi-humid clay soil	1200	1.5 [16]

2.2. Liquid Materials

For thermal energy storage in high temperature liquid media there is a lot of experience in the use of molten salts for the heat treatment industry and in concentrated solar power plants (solar towers). The advantages of molten salts are its thermal stability, relatively low material costs, heat capacity, high density, non-flammability and low vapor pressure. Because of this low vapor pressure, pressurized vessels are not required, substantially reducing tank costs. Other high temperature storage fluid options

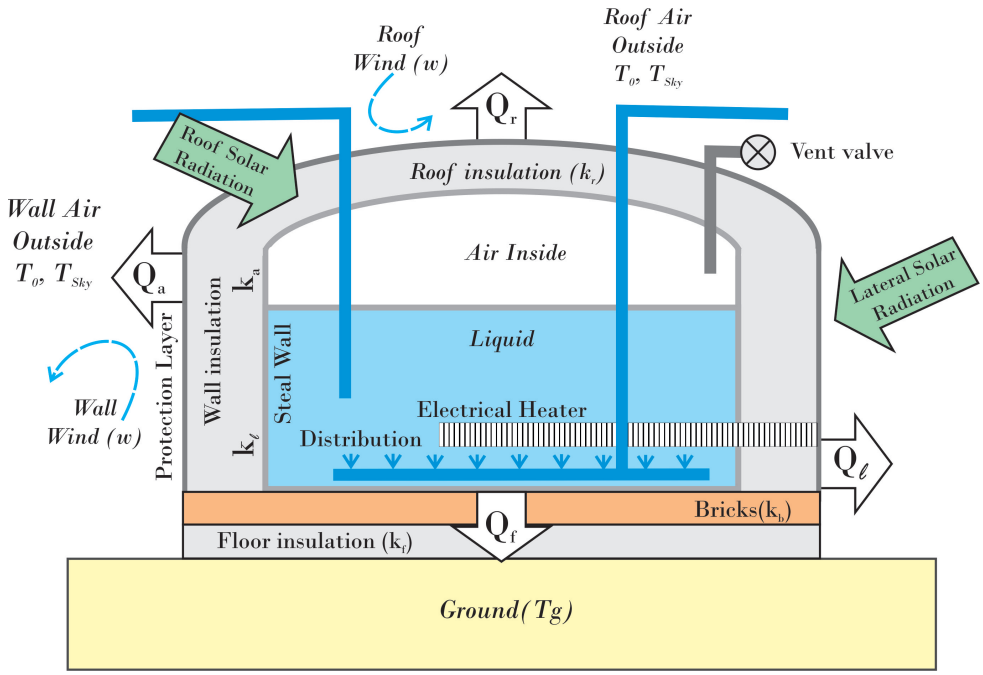

Figure 3: Schematic model of a thermal tank for PHES applications, ambient factors and heat leak losses.

include ethylene glycol, mineral, synthetic or organic oils, some eutectic salts, and liquid metals such as sodium [3, 17].

Commercial solar salt is basically composed of nitrates (60% $NaNO_3$ y 40% KNO_3), but there is a wide variety that can be used for PHES. The temperature ranges for the use of commercial salt involve a maximum associated with thermal decomposition limitation that happens in the range of 870K and a minimum corresponding to the melting point, which is around 520K, therefore, when designing this type of system, it is necessary to take a certain margin of safety in the definition of the operating parameters.

The physical properties of the commercial solar salt are adjusted with temperature with the equations in Table 2.

Table 2: Properties of the molten salt with temperature (in K) [14].

Conductivity (W/mK)	$0.3911 + 1.9{\cdot}10^{-4}T_S$
Viscosity (kg/ms)	$7.55.10^{-2} - 2.78{\cdot}10^{-2}T_S + 3.49{\cdot}10^{-7}T_S^2 - 1.47{\cdot}10^{-10}T_S^3$
Density (kg/m^3)	$2236.72 - 0.636T_S$
Isobaric expansion coef.	$0.636/(2263.72 - 0.636T_S)$
Specific heat (J/kgK)	$1396 + 0.172T_S$

About to cold liquids, mixtures of eutectic brine and ice have been used [18]. Other authors suggest hydrocarbons or alcohols (methanol or ethanol), since these fluids remain liquid between 180 K and 300 K with a vapor pressure of less than 1 atmosphere. Lower alcohols such as methanol, ethanol, propanol, and propylene glycol are hygroscopic and become viscous at cold temperatures when mixed with water, so humidity control will be necessary [4]. Among the alcohols, methanol is relatively cheap, available in local market, and used by the chemical industry. Cold storage with methanol does not present major risks provided it is kept below boiling temperature and standard precautions are taken about its flammability and toxicity. In that regard, this article takes as a reference the use of methanol as a cold fluid. Its properties associated to various parameters such as pressure and temperature are available through the Coolprop [**?**] software coupled to Octave [19].

2.3. Round trip efficiency

In most cases, considering heat pump or engine, there is a direct heat transfer with the environment and even from the hot source to the cold one through the plant itself. This heat transfer is related to the heat losses that always take place between the hottest and coldest parts of any area of the installation through the components of the plant and its walls [20]. Generally and in the short term they can be considered negligible since, in principle, any insulation thickness can be achieved [21]. However, the high tank temperatures and long waiting hours between charging-discharging cycles must be considered for their effects on stored energy.

The losses to the surrounding environment affect the temperature of the stored salts and cold liquid. The effect is to reduce T_{H1} and T_{H2} and to increase T_{L1} and T_{L2}. The impact of irreversibility in the cold reservoir is small, because its temperatures are close to the ambient temperature and the conductivity of the insulators is lower, it will not decrease as much the round trip efficiency as the high temperature reservoir.

Considering a linear model, the effect on the temperatures of

the molten salt and methanol reservoirs will be [2]:

$$T^{HE}_{H1f} = T^{HE}_{H10} - \xi_{Hs}(T^{HE}_{H10} - T_0) \quad \text{Storage and discharge time.} \quad (4)$$

$$T^{HE}_{L1f} = T^{HE}_{L10} + \xi_{Ls}(T_0 - T^{HP}_{H20}) \quad \text{Storage and discharge time.} \quad (5)$$

$$T^{HP}_{H2f} = T^{HP}_{H20} - \xi_{Hw}(T^{HP}_{H20} - T_0) \quad \text{Waiting and charge time.} \quad (6)$$

With ξ_i equal to the heat leak coefficient for the solar salt and methanol storage tanks and for the waiting tank.

Since the heat leak affects only the heat transfers and that the round trip efficiency is defined by the work relationship between the charge and discharge cycle, there would not be clear the order of magnitude of this irreversibility effect. Therefore, the impact on the temperatures of the high and low reservoirs is what will reflect the impact of these thermal leaks.

As with other loss coefficients, these terms are integrated over time, remembering that heat leak losses occur during the charging, discharging, waiting and storage phases (24 hours per day).

The coefficient of performance for the heat pump cycle (ν_{HP}), the efficiency of the heat engine cycle (η_{HE}) and the RTE of the global cycle system are quantified according to the model developed by Salomone et al. [2]. The equations are described below:

$$\nu_{HP} = \frac{Z_2\left(\frac{1-\epsilon_L}{\epsilon_L}\right) - \frac{1}{Z-1\epsilon_L} + \frac{T^{HP}_{L2}}{T^{HP}_{H2}}}{Z_2\left(\frac{1-\epsilon_L}{\epsilon_L} + \frac{T^{HP}_{L2}}{T^{HP}_{H2}}\frac{1-\epsilon_H}{\epsilon_H}\right) + \frac{Z_2}{Z_1} - \frac{1}{Z_1}\left(\frac{1}{\epsilon_H} + \frac{1}{\epsilon_L}\right) + \frac{T^{HP}_{L2}}{T^{HP}_{H2}}} \quad (7)$$

$$\eta_{HE} = 1 + \left[\frac{T^{HE}_{L1}\epsilon_L(Y_1Y_2(1-\epsilon_H) - 1) + T^{HE}_{H1}Y_2\epsilon_H\epsilon_L}{T^{HE}_{H1}\epsilon_H(Y_1Y_2(1-\epsilon_L) - 1) + T^{HE}_{L1}Y_1\epsilon_H\epsilon_L}\right] \quad (8)$$

$$RTE = \frac{\eta_{HE}Q^{HE}_H}{\nu^{-}_{HP}1Q^{HP}_H} \quad (9)$$

For the heat pump cycle:

$$Z_1 = \frac{r^{(\gamma-1)/\gamma}_{cHP} - (1-\epsilon_c)}{\epsilon_c} \quad \text{and} \quad Z_2 = \frac{r^{(\gamma-1)/\gamma}_{tHP}(1-\epsilon_t) + \epsilon_t}{r^{(\gamma-1)/\gamma}_{tHP}}$$

and for the heat engine cycle:

$$Y_1 = \frac{r^{(\gamma-1)/\gamma}_{cHE} - (1-\epsilon_c)}{\epsilon_c} \quad \text{and} \quad Y_2 = \frac{r^{(\gamma-1)/\gamma}_{tHE}(1-\epsilon_t) + \epsilon_t}{r^{(\gamma-1)/\gamma}_{tHE}}$$

with r_c the compression ratio and r_t the expansion ratio for the turbine (which are different for charge and discharge cycles). ϵ_c and ϵ_t are equivalent to the isentropic efficiency of the compressor and the turbine respectively. ϵ_H and ϵ_L are the global effectivenesses of high and low pressure heat exchangers.

The heat flows in the high-pressure reservoirs are:

$$Q^{HP}_H = C_H(T^{HP}_{H1} - T^{HP}_{H2}) \quad \text{and} \quad Q^{HE}_H = C_H(T^{HE}_{H1} - T^{HE}_{H2})$$

Pressure drops of the fluid along the hot and cold sides are ΔP_H and ΔP_L, so that for the heat pump cycle:

$$r_{cHP} = P_{1HP}/(P_{3HP} - \Delta P_L) \quad \text{and} \quad r_{tHP} = (P_{1HP} - \Delta P_H)/P_{3HP}$$

and for the heat engine cycle:

$$r_{cHE} = P_{2HE}/(P_{4HE} - \Delta P_L) \quad \text{and} \quad r_{tHE} = (P_{2HE} - \Delta P_H)/P_{4HE}$$

The contained mass (M_i) of heat transfer fluid (hot and cold) will be given by:

$$M_H = \frac{\dot{m}_w c_{pw} t_i}{c_{pH}\Gamma_H} \quad \text{and} \quad M_L = \frac{\dot{m}_w c_{pw} t_i}{c_{pL}\Gamma_L} \quad (10)$$

Where M_H is the molten salt mass and M_L is the cold fluid mass. $\dot{m}_w$ is the flow of the working gas. c_{pH} and c_{pL} are the specific heats of the hot and cold fluids. t_i is the charging or discharging time depending on the required capacity. The values of Γ_i are:

$$\Gamma_H = \frac{C_w}{C_H} < 1 \quad \text{and} \quad \Gamma_L = \frac{C_w}{C_L} < 1 \quad (11)$$

Where C_w, C_H and C_L are the heat capacities of the working, storage and cold fluid ($C = \dot{m}c_p$).

Using these equations and the reservoir temperatures adjusted from the heat leak losses, the temporary loss will be associated with the RTE performance of the PHES technology.

3. Heat leak model.

During the waiting periods (before charging) and storage (after charging), one of the two tanks (both in the hot and cold zone) will be full, then, the loss will be considered from a constant liquid level, consequently, from a constant lateral surface. During charging or discharging, the tanks also lose energy, but at a variable heat transfer and leakage area. While it can be neglected, since charging and discharging times are usually considerably shorter than storage and waiting times, a heat leak can be calculated associated with each level that influences the resulting temperature at the end of the process. The proposed model is developed assuming that the tanks are completely emptied after each period. However, it should be clarified that the probable remnant that remains in the pipe may require additional heating to avoid the crystallization of the solar salts.

The calculation procedure for the heat loses of one tank is presented below, but it is analogous for the other tanks.

Net heat loss Q_n, that cause molten salt to cool and methanol to heat, can be subdivided into four main components: losses through the ground Q_f, through the roof Q_r, through the wall in contact with the air over the liquid Q_a and through the wall in contact with the liquid Q_ℓ [22].

$$Q_n = Q_f + Q_r + Q_a + Q_\ell \quad (12)$$

Beyond the reservoir design itself, losses will depend on the local climatic conditions where the system is installed. Calculations must necessarily be associated with factors such as ambient, ground and sky temperature, surrounding wind speed and incident solar irradiation (determined from available parameters such as horizontal radiation, brightness index, direct ratio and different solar angles for each hour of the day).

The analysis of the thermal behavior of a tank exposed to the environment requires a complex analysis of transient heat transfer, since the temperature of the liquid does not depend only on the outward heat losses, but also on the heat leak to the surrounding air at atmospheric pressure above the liquid (the air contained in the tank occupying the empty volume) [8, 23, 24].

The different heat flows that compose the tank losses for the waiting and storage tanks can be seen in the Fig. 4a and are associated with:

- Internal convection between the liquid and the air in contact inside the tank ($Q_{Ca\ell}$).-
- Internal convection between liquid and walls - Lateral ($Q_{C\ell i}$) and floor (Q_{Cfi}).-
- Internal convection between the internal air over the liquid and the walls - Lateral (Q_{Cai}) and roof (Q_{Cri}).-
- External forced or natural convection between the ambient air and the outer wall - Roof (Q_{Cr0}) and walls (Q_{Ca0} and $Q_{C\ell 0}$).-
- Conduction through metal walls, thermal insulation and external protections - Roof (Q_{Kr}), floor (Q_{Kf}), wall (Q_{Ka} and $Q_{K\ell}$).-
- Conduction through the ground (Q_{Kg}).-
- Radiation from lateral walls and roof to the exterior - Roof (Q_{Rr0}) and walls (Q_{Ra0} and $Q_{R\ell 0}$).-
- Outgoing radiation from the liquid surface ($Q_{R\ell\ell}$) to the lateral wall (Q_{Rai}) and roof (Q_{Rri}).-
- Incident solar radiation - Roof (Q_{Gr}) and lateral walls ($Q_{G\ell}$) and (Q_{Ga}).-

In the scheme it can be seen that, unlike the roof and floor, the heat transfer model through the lateral walls is divided into two paths, always in the direction normal to the heat flow. Thus, the model considers the level in the PHES tank, therefore, a different thermal losses must be assigned to both zones, associated to the volume of liquid and the volume of air inside the tank. It is important to note that in this model, the liquid surface temperature, in contact to the air, is equal to the entire liquid.

An approximate profile of the temperature along the length and height of the tank can be seen in the Fig. 4b, where the liquid temperature (T_ℓ), internal air (T_a), the inside and outside lateral wall in contact with the air (T_{ai} and T_{a0}), the inside and outside lateral wall in contact with the liquid ($T_{\ell i}$ and $T_{\ell 0}$), the inside and outside of the floor (T_{fi} and T_{f0}) inside and outside of the roof (T_{ri} and T_{r0}). T_0, T_{sky} and T_g are the ambient, sky and ground temperature are indicated. Furthermore, H is the inside height of the tank, z is the fluid level and D is the diameter. e_i is the wall thickness including steel, insulation and protective layer (the outside diameter is $D_0 = D + 2e$). For the case of methanol, as the energy flows in the opposite direction, instead of a decrease there is an increase in temperature.

It is clear that each influencing factors have different levels of impact and in many cases, they are negligible with respect to each other. To estimate this influence, based on the nomenclature shown in Fig. 4a, it is noted that the heat losses are composed of different transfer processes, whose balances are described below:

Lateral wall - Liquid zone balance

$$Q_\ell = Q_{C\ell i} = Q_{K\ell} = Q_{C\ell 0} + Q_{R\ell 0} - Q_{G\ell} \tag{13}$$

Roof balance

$$Q_r = Q_{Rri} + Q_{Cri} = Q_{Kr} = Q_{Cr0} + Q_{Rr0} - Q_{Gr} \tag{14}$$

Floor balance

$$Q_f = Q_{Cfi} = Q_{Kf} = Q_{Kg} \tag{15}$$

Lateral wall - Air zone balance

$$Q_a = Q_{Cai} + Q_{Rai} = Q_{Ka} = Q_{ca0} + Q_{Ra0} - Q_{Ga} \tag{16}$$

In addition:

$$Q_{Ca\ell} = Q_{Cri} + Q_{Cai} \qquad \text{and} \qquad Q_{R\ell i} = Q_{Rri} + Q_{Rai} \tag{17}$$

To simplify, only the hot tank situation is presented, but for the cold tanks the equations are the same although, in this case, the heat is entering.

Each of these heat flows and their respective calculation method are described below.

3.1. Convective mechanisms

The convective heat transfer in the different media (solar salt, methanol, air above the liquid and outside air) (Q_{cx}) is determined by the equation 18:

$$Q_{cx} = h_{cx}(T_{Hx} - T_{Lx})A_x \quad \text{with} \quad h_{cx} = \frac{k_x Nu_x}{L_x} \tag{18}$$

T_{Hx} is the higher temperature, T_{Lx} is the lower temperature, A_x is the transfer area and h_{cx} is the convective heat transfer coefficient obtained from the dimensionless correlations from the Nusselt number (Nu) which for natural convection is a function of the Prandtl number (Pr) and the Grashof number (Gr) and for forced convection depends on the Prandtl number and the Reynols number (Re). Therefore, $Nu = f(Pr, Gr, Re)$. In all cases, the properties of the fluids involved in convective mechanisms are analyzed at the film temperature, $T_{film} = 1/2(T_H - T_L)$ [25]. Table 3 describes the different correlations for the calculation of the Nusselt, Grashof, Prandtl and Reynolds number.

A_x is calculated according to $A_\ell = \pi Dz$ for the cylinder in the lower area of the tank in contact with the liquid, $A_a = \pi D(H-z)$ for the upper cylinder area and for the lids (floor and roof) it is calculated as $A_{rf} = \pi D^2/4$. For the outer lateral walls the outer diameter (D_0) is used for the convective coefficient calculations.

On external surfaces (lateral and roof), where the incidence of wind speed (w) must be taken account, the ratio between the Grashof number and the Reynolds number squared (Gr/Re^2), indicates whether natural or forced convection dominates the

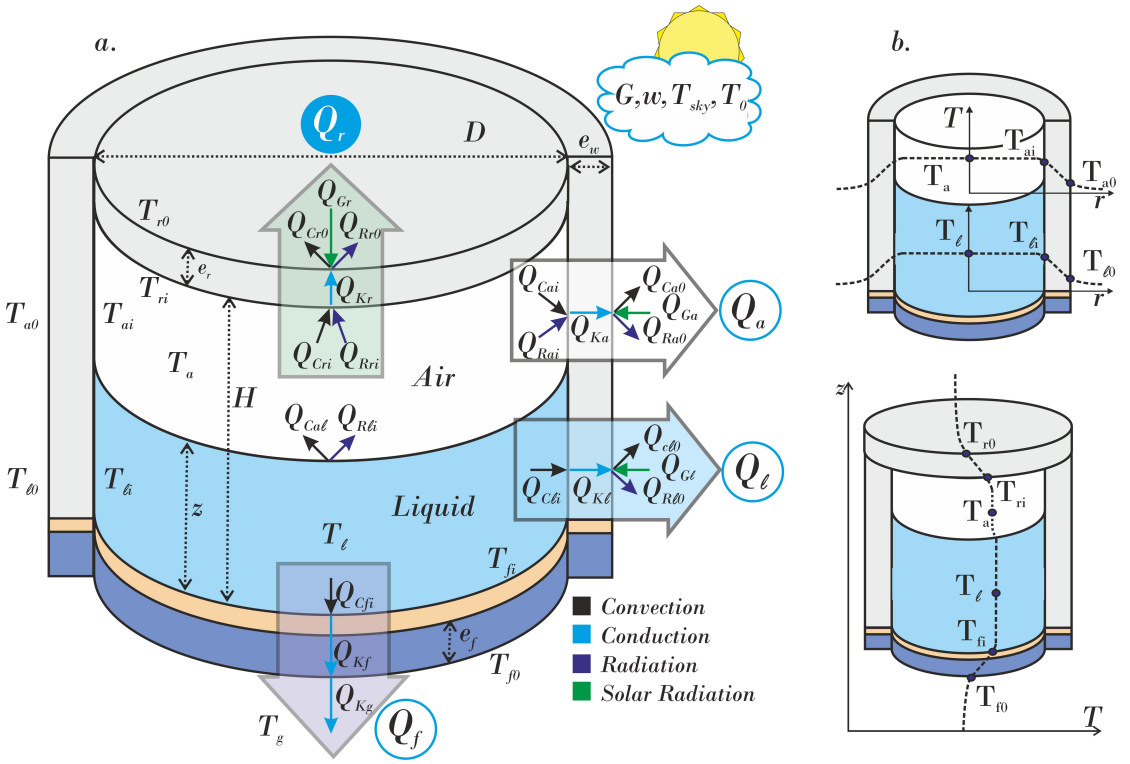

Figure 4: (a) Tank model scheme and and heat flows (b) Temperature distributions. For cold tank (methanol), except to radiative heat transfer at the tank's outer surface (Q_{Gx}), all heat flows have the opposite direction

heat transfer. Therefore, depending on this ratio, one has that the weighted convection coefficient is defined as [25, 26]:

$$h = sh_n + (1 - s)h_f \tag{19}$$

$$\begin{aligned} s &= 0 \quad \text{for turbulent flow with} \quad Gr/Re^2 < 0.7 \\ s &= f(Gr/Re^2) \quad \text{for mixed flow with} \quad 0.7 \leq Gr/Re^2 \leq 10 \\ s &= 1 \quad \text{for laminar flow with} \quad Gr/Re^2 > 10 \end{aligned}$$

h_n is the natural convection coefficient, h_f is the forced convection coefficient and s is the relative fraction of each one. In case the ratio is in the range $0.7 \leq \mathrm{Gr/Re^2} \leq 10$ a linear variation will be assumed to perform the calculations, where f=0 for $\mathrm{Gr/Re^2}$=0.7 and f=1 for $\mathrm{Gr/Re^2}$=10.

3.2. Conductive mechanisms

On the lateral walls should use the cylindrical conduction model and on the horizontal walls (roof and floor) the one-dimensional flat multilayer conduction format. There will also be a heat transfer between the external wall of the tank floor and the ground. For this mechanism, it is assumed that conduction happens between an isothermal disk at a different temperature concerning the semi-infinite medium at a location away from the disk [25]. The equations associated with each mechanism are described in the Table 4.

3.3. Radiation mechanisms

For external radiation heat transfer, the exchange with the environment is taken considering the environment as a black body. The limiting temperature of the black body is set to the sky temperature T_{sky} and the Stefan-Boltzmann formulation described in Table 5 for each surface (considered as gray opaque diffuse surfaces, with equals absorptivity and emissivity). As far as internal radiation, a heat exchange is assumed in the cavity formed between the liquid surface and the non-wetted parts of the inner wall of the steel (roof and dry wall). The three corresponding surfaces are then considered; the liquid surface (cold fluid or solar salt), the surface of the tank roof and the surface of the tank wall in contact with the internal air with cylindrical shape. The heat transfer by radiation between surfaces depends on the orientation of the areas to each other, as well as on their properties and temperatures. To take the effects of surface orientation on the radiative heat transfer between two walls, it takes the parameter called shape factor (F_{ij}), which is a purely geometrical quantity, independent of material properties and temperature. This factor is equivalent to the fraction of the radiation leaving surface i and arriving directly at surface j [26]. The equations for calculating each shape factor result:

$$F_{\ell r} = \frac{1}{2}\left(S - \left[S^2 - 4\right]^{1/2}\right) \quad \text{with} \quad S = 1 + \frac{1 + \left(\frac{r_i}{H - z}\right)^2}{\left(\frac{r_i}{H - z}\right)^2} \tag{20}$$

From which the other shape factors can be deduced, such as $F_{r\ell} = F_{\ell r}, F_{ra} = 1 - F_{r\ell}, F_{\ell a} = F_{ra}, F_{ar} = F_{ra}(A_{rf}/A_a)$ and $F_{a\ell} = F_{ar}$.

For the calculation of internal radiation losses, it takes the cylinder with three opaque and diffuse gray surfaces in the area

Table 3: Empirical correlations for the average Nusselt number for natural and forced convection over surfaces. Correlations for Grashof, Prandtl and Reynolds numbers. μ_i is the viscosity, $c_{p,i}$ is the specific heat, k_i is the conductivity, g is the acceleration due to gravity ($9.81 m/s^2$), L is the characteristic length and i_e is the isobaric expansion coefficient. ν is the cinematic viscosity such that $\nu = \mu/\rho$ [26].

Natural Convection						
Zone	*Nu*	*Range*	Q_{Cx}	L_x	T_{Hx}	T_{Lx}
Lateral wall	$1.36(GrPr)^{1/5}$ $0.55(GrPr)^{1/4}$ $0.13(GrPr)^{1/3}$	$GrPr < 10^4$ $10^4 < GrPr < 10^9$ $GrPr > 10^9$	$Q_{C\ell i}$ $Q_{C\ell 0}$ Q_{Cai} Q_{Ca0}	z z $H-z$ $H-z$	T_ℓ $T_{\ell 0}$ T_a T_{a0}	$T_{\ell i}$ T_0 T_{ai} T_0
Horizontal wall Hot down	$0.27(GrPr)^{1/4}$	$10^5 < GrPr < 10^{11}$	$Q_{Ca\ell}$ Q_{Cri} Q_{Cr0}	$D/4$ $D/4$ $D/4$	T_ℓ T_a T_{r0}	T_a T_{ri} T_0
Horizontal wall Hot up	$0.54(GrPr)^{1/4}$ $0.14(GrPr)^{1/3}$	$10^5 < GrPr < 10^7$ $10^7 < GrPr < 10^{10}$	Q_{Cfi}	$D/4$	T_ℓ	T_{fi}
Forced Convection						
Lateral wall	$0.3 + \frac{0.62Re^{1/2}Pr^{1/3}}{\left(1+\left(\frac{0.4}{Pr}\right)^{2/3}\right)^{1/4}} \times ...$ $... \left[1+\left(\frac{Re}{282.000}\right)^{5/8}\right]^{4/5}$	–	$Q_{C\ell 0}$ Q_{Ca0}	D D	$T_{\ell 0}$ T_{a0}	T_0 T_0
Horizontal wall Hot down	$0.664Re^{1/2}Pr^{1/3}$ $0.037Re^{0.8}Pr^{1/3}$	$Re < 5x10^5$ $Pr > 0.6$ $5x10^5 < Re < 10^7$ $Pr > 0.6$	Q_{Cfi}	D	T_{fi}	T_ℓ
Numbers						
Grashof (Gr)	$\frac{g\rho_i^2 i_e(\lvert T_H - T_L\rvert)L^3}{\mu_i^2}$	*Prandtl(Pr)*	$\frac{\mu_i c_{pi}}{k_i}$	*Reynolds (Re)*		$\frac{wL}{\nu}$

occupied by the air between the inside roof (r), the lateral wall (a) and the liquid (ℓ). Such a cylinder has surface areas A_a, A_r and A_ℓ ($A_r = A_\ell = A_{rf}$) ; emissivities ε_r, ε_a, and ε_ℓ and temperatures T_{ri}, T_{ai} and T_ℓ, respectively. An equivalent electrical radiation scheme of this geometry is shown in Fig. 5 where E_{br}, E_{ba} and $E_{b\ell}$ are the potentials specified at the surface temperature (equivalent to blackbody emissive power, $E_b = \sigma T^4$) and the radiosities J_r, J_a and J_ℓ are the unknowns. The three equations for the determination of these three unknowns are obtained from the requirement that the algebraic sum of the currents (net radiative heat transfer) at each node must equal zero.

From the scheme in Fig. 5, the three equations to determinate the three unknowns are obtained from the equality to zero of the sum of the currents (net radiative heat transfer) at each node.

$$\frac{(E_{br} - J_r)A_r\epsilon_r}{1-\epsilon_r} + A_rF_{ra}(J_a - J_r) + A_rF_{r\ell}(J_\ell - J_r) = 0 \quad (21)$$

$$\frac{(E_{ba} - J_a)A_a\epsilon_a}{1-\epsilon_a} + A_aF_{ra}(J_r - J_a) + A_aF_{a\ell}(J_\ell - J_a) = 0 \quad (22)$$

$$\frac{(E_{b\ell} - J_\ell)A_\ell\epsilon_\ell}{1-\epsilon_\ell} + A_\ell F_{r\ell}(J_r - J_\ell) + A_aF_{a\ell}(J_a - J_\ell) = 0 \quad (23)$$

The simplification used for the calculations can be seen in Table 5.

Table 4: Correlations for conductive mechanisms Q_i. k_i is the multilayer conductivity and e is the wall thickness and the shape ground factor $S = 2D$. $L = z$ to $Q_{K\ell}$ and $L = H - z$ to Q_{Ka}

Conduction				
Zone	*Q*	Q_{Kx}	T_{Hx}	T_{Lx}
Lateral wall [26]	$2\pi Lk_i\,[(T_H - T_L)/ln(D_0/D)]$	$Q_{K\ell}$ Q_{Ka}	$T_{\ell i}$ T_{ai}	$T_{\ell 0}$ T_{a0}
Horizontal wall [26]	$k_i/e(T_H - T_L)A_{fr}$	Q_{Kr} Q_{Kf}	T_{ri} T_{fi}	T_{r0} T_{f0}
Ground [28]	$Sk_g(T_{fe} - T_g)$	Q_{Kg}	T_{f0}	T_g

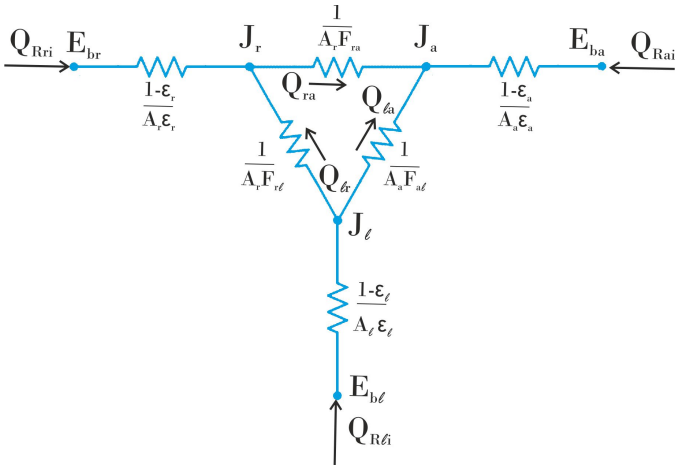

Figure 5: Radiation network associated to a three-surface enclosure cylinder PHES.

3.4. Incident solar radiation

Considering the incident solar irradiance (Q_{Gi}), as the reservoirs are usually located outdoors, the external protective layer is exposed to solar irradiance during the morning and afternoon and therefore, the tank is exposed to large daily temperature fluctuations. The absorbed solar through the wall and roof influences in favor the RTE in high temperature tanks and against it in low temperature tanks [8].

Generally, the irradiation measurements obtained from meteorological stations are global values on the horizontal plane, but the incident irradiation on the lateral surface is not horizontal, so it is necessary to use some method of adjustment by analyzing the angle of incidence on the exposed area.

Incident irradiance over an inclined surface can be calculated as the sum of four components [27]:

$$G_n = G_{bi} + G_{dic} + G_{dii} + G_{ri} \tag{24}$$

Where G_n represent the net radiation over the inclined plane and G_{bi} the direct, G_{dic} the circumsolar diffuse, G_{dii} is the isotropic diffuse and G_{ri} is the reflected.

Table 5: Correlations for radiative mechanisms Q_i. σ_B is the Stefan–Boltzmann constant equivalent to $5.67 \times 10^{-8} W/(m^2K^4)$. ε_x is the surface emissivity for each material. J_x is the radiosity for each layer. T_{sky} depends on atmospheric conditions and covers a range that goes from the order of 230K for a cold and clear day to 285K for a warm and cloudy day. T_i is the temperature for each material [26].

External Radiation					
Zone	Q_r	Q_{rx}	T_H	T_L	A_x
External Lateral Wall	$A_x\sigma_B\varepsilon_0(T_H^4 - T_{sky}^4)$	$Q_{R\ell 0}$ Q_{Ra0}	$T_{\ell 0}$ T_{a0}	T_{sky} T_{sky}	A_s A_a
External Roof		Q_{Rr0}	T_{r0}	T_{sky}	A_{rf}
Internal Radiation					
Zone	Q_r			Q_{rx}	A_x
Internal roof	$A_x\epsilon_r(J_r - \sigma_B T_{ri}^4)/(1 - \epsilon_r)$			Q_{Rri}	A_{fr}
Liquid surface	$A_x\epsilon_\ell(J_\ell - \sigma_B T_\ell^4)/(1 - \epsilon_\ell)$			$Q_{R\ell i}$	A_{fr}
Internal Lateral Wall	$A_x\epsilon_a(J_a - \sigma_B T_{ai}^4)/(1 - \epsilon_a)$			Q_{Rai}	A_a

Diffuse fraction is $f_d = G_{dh}/G_h$ and depends on an index of clarity κ_T which, in the absence of historical data, can be determined according to the Ruiz Arias correlation [27]:

$$f_d = a_0 + a_1 e^{e^{(a_2 + a_3\kappa_T)}} \tag{25}$$

With $a_0 = 0.952$, $a_1 = -1.041$, $a_2 = 2.300$, $a_3 = -4.702$. The geometric factor b (direct ratio) is also defined and relating the hourly direct irradiation on the lateral surface and the horizontal one. $b = G_{di}/G_{bi} = \cos\theta/\cos\theta_z$. Where θ_z is the zenith angle (formed by the earth-sun line with the vertical at the observer's point) and θ is the angle of incidence formed by the direct solar radiation (ground-sun line) with the normal to the tank wall. Both angles depend on the position of the sun for the selected time and location of the system PHES. For this reason, the incidence of this factor varies during the course of the day.

The incident solar irradiance for the lateral wall is considered using the equations below [27]:

$$\begin{aligned} G_{bi} &= G_{bh}b \\ G_{dic} &= bT_bG_{dh} \\ G_{dii} &= G_{dh}(1 - T_b)\left(\frac{1 + cos\delta}{2}\right) \\ G_{ri} &= G_h\rho_g\left(\frac{1 - cos\delta}{2}\right) \end{aligned} \tag{26}$$

ρ_g is the floor reflectivity and T_b is the atmospheric trasmisivity which is calculated as $T_b = (1 - f_d)\kappa_T$.

The heat absorbed by the lateral walls, taking into account the projected area since it is not a flat surface, results then:

$$Q_{G\ell} = G_{n\ell}zD_0a_s \qquad \text{and} \qquad Q_{Ga} = G_{na}(H - z)D_0a_s \tag{27}$$

Where a_s represents the absorptivity of the wall, δ is the inclination which is always 90°.

Solar irradiation on horizontal roofs is calculated as follows [27]:

$$Q_{Gr} = (G_{bh}cos\theta_z + G_{dh})A_{fr}a_s \quad (28)$$

3.5. Results

Heat leak (in this work understood as the loss to the environment), will depend essentially on the isolation of the reservoirs and the external conditions associated with the climate of the area where the PHES tank are installed. In this section, the different influences of these parameters on the RTE are evaluated.

For the analysis it was considered that for the inside air as well as for the liquid contained into the tanks (solar salt or methanol) there is a uniform temperature distribution throughout the reservoir including the liquid surface exposed to the air. It is only taken into account that the liquid volume has a small gradient near the interfaces with the tank steel, but essentially, the liquid is homogeneous including the surface in contact with the air above the liquid.

During storage, the high temperature tank (T_{H1}) and the low temperature methanol tank (T_{L1}) will be full, with a safety margin occupied by air above the liquid (assumed for calculations in the order of 10%). In that period, the waiting tanks may be totally or practically empty, with a bottom limited by the salt inlet height to the tank and the heating resistors. In this article, it is assumed that the plant size is adjusted to the times that allow the tanks to be completely emptied to avoid crystallization of salts in the bottom remnant. After the discharge stage, during the waiting period for surplus power, the methanol and solar salt storage tanks will be empty and the waiting tanks will remain full at T_{H2} and T_{L2}.

The properties of the solar salt correspond to the correlations presented in Table 2. For the properties of methanol and air, the Octave program [19] is associated with data from the Coolprop software [**?**].

This work takes as reference the case of a system consisting of Argon, commercial solar salt and methanol, located in a city with a subtropical wet weather (although it can be adjusted to any community based on climatic data) for a net production of 5 MW of electrical power. Steel tanks with mineral wool insulation for walls and roof are proposed. There will be foam glass for floors and a 15 cm fixed refractory brick layer. For the methanol tank, the same insulation will be used for the floors and polyurethane foam for the walls. The conductivity of each material present is determined according to the equations in Table 1. The storage temperature (T_{H1}) is assumed 850 K and the waiting tank (T_{H2}) is 550 K. The methanol tank low temperature (T_{L1}) is 250 K at the beginning of the discharge and at the end (T_{L2}) it will have a maximum of 330K. Applying the equations of the finite-time thermodynamics model described by Salomone et al. [2], the dimensional characteristics of the Table 6 are determined and the round trip efficiency will be calculated. The main numerical routine is setted with hourly frequency input climate parameters ($T_0, T_{sky}, T_g, G_{bh}, G_{dh}, w, cos\theta, cos\theta_z, \kappa_T$ and b), depending on the day of origin of the simulation (data 1 is the first day of summer), input parameters such as the z/D ratio and the insulation thickness and with them the results are obtained by solving a system of equations. Then, the variables are updated, the temperature data for the wall, floors and roofs, interior and exterior, are obtained and the system is rerun until convergence is achieved iteratively. A 5-hour charging and discharging time is assumed to fix the storage capacity.

Table 6: Operating data - PHES Molten Salt-Methanol-Argon - 5MW

Operational conditions			
$T_{H1}(K) = 850$	$T_{H2}(K) = 550$	$T_{L1}(K) = 250$	$T_{L2}(K) = 330/300$
$P_{min}(MPa) = 0.1$	$r_c^{HP} = 12.4$	$r_c^{HE} = 4.2$	$\Delta_{Pi} = 0.01$
$\epsilon_H = 0.95$	$\epsilon_L = 0.90$	$\epsilon_c = 0.90$	$\epsilon_t = 0.90$
$c_{pg}(kJ/kgK) = 0.52$	$\dot{m}_g(kg/s) = 111.4$	$k = 0.4012$	$t_{c,d}(h) = 5$
$\Gamma_H = 1.00$	$\Gamma_L = 0.35$	$M_H(ton) = 687$	$M_L(ton) = 1198$

As mentioned above, to know the relative impact of each of the mechanisms, the historical wind speed, ambient air temperature and incident solar irradiation on the tanks must be taken into account. The ground temperature is quite stable for the selected area and is close to the annual average ambient temperature. Sky temperature is assumed in 253K.

As shown in Fig. 6, for a city with subtropical wet weather, the ambient temperature, wind and radiation vary from day or night, winter to summer, affecting the losses depending on the storage period at the implementation area.

In this article, the emissivity of 0.33 is considered as a reference for the inside faces of the stainless steel tank [28]. The ground emissivity at near ambient temperatures, for a protection layer of the tank in oxidized galvanized steel sheet, is equivalent to 0.28 [28]. Finally the surface of the molten salts is considered as a black body of emissivity 1 [29].

For the external direct radiation, the solar absorptivity of the galvanized layer is taken to be 0.80 and the ground reflactance (ρ_g) is assumed to be 0.26 for a green grass floor [27].

The different influencing factors will be evaluated below in order to understand the behavior of the system for different situations.

Considering the tank geometry, the effect over the final temperature in the tanks was previously studied, varying the z/D ratio and for value of approximately 0.65 for both tanks obtained the best values.

Fig. 7 shows the average fractions of heat loss or absorption for tanks filled with commercial solar salt and methanol during storage and waiting for one summer and winter month. As can be seen, the most important heat transfer is through the lateral walls. More than 50% of the energy is lost between the walls in contact with the external air. The losses through the ground remains practically constant (because of the temperature stability of the ground) and its relative influence is greater in the

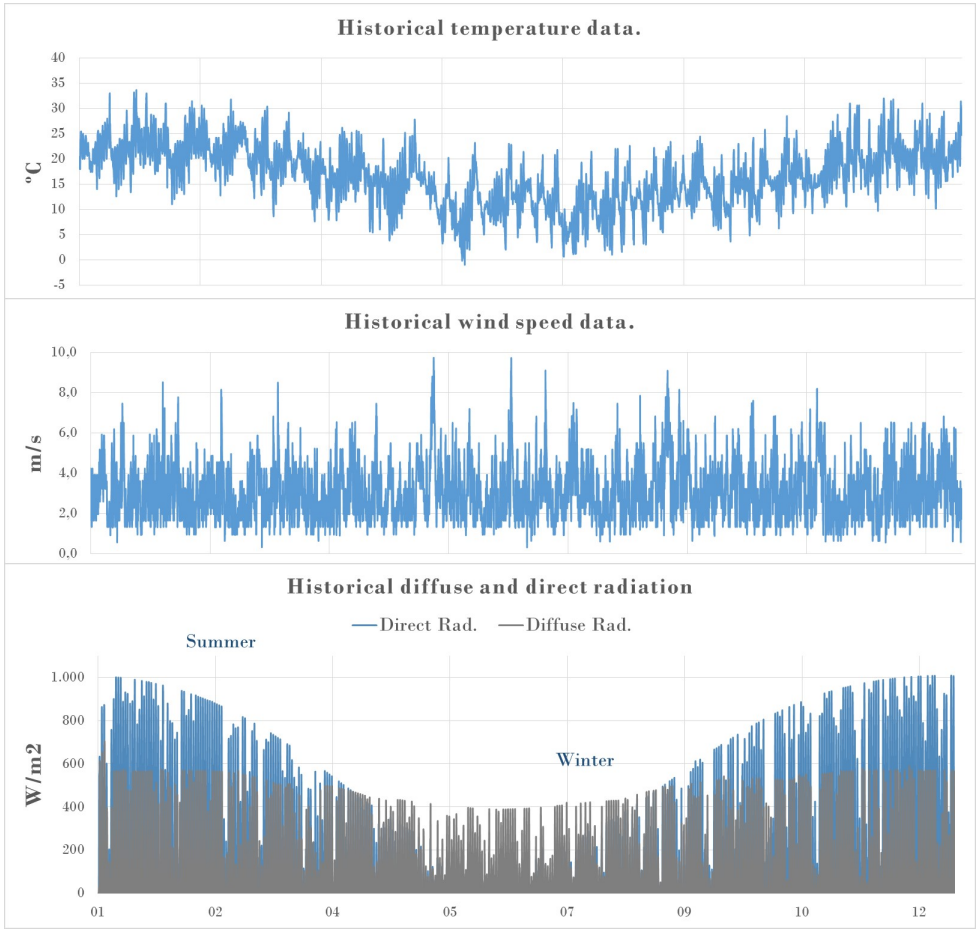

Figure 6: Annual variation of ambient air temperature, wind speed and solar irradiation (direct and diffuse) for a reference city with subtropical wet weather. Day 1=Summer [30].

methanol tank, mainly because of the smaller effect of external radiation as the temperature inside the tank resembles the T_{sky}.

Comparatively, the heat losses rates for tanks with elevated operating temperatures were higher as the thermal gradient between the storage material and the environment is larger, resulting in higher heat exchange. This goes against the benefits of PHES since the higher temperature, there are more storage capacity, more power available and higher RTE. Methanol heating is also detrimental when evaluating RTE performance, but it does not influence drastically [2].

As far as the variations in climatic conditions, high temperature tanks are more relative affected in winter and low temperature tanks in summer. However, there is not much difference between cold and summer climates for hot tanks. It is noted that when the temperature of the contained liquid is lower, the relative effect is clearer. The variation of the seasonal loss on the storage tanks (at T_{H1}) is some 1% between winter and summer, 3% for the waiting tank (at T_{H2}) and more than 20% for the methanol tank (at T_{L1}). The higher variation is then in the cold tank and although its influence on the RTE is lower, the possible small differences in performance between winter and summer will be especially due to this effect on the methanol temperature. The high frequency variation are caused by daily fluctuations in weather conditions.

In Fig. 8 the heat leak coefficient described in the equation 6 is plotted for periods of one month in the worst possible condition (winter in high reservoirs and summer in low reservoirs). It is noted that in all tanks that the losses increase with time for different insulation thicknesses. As expected, the loss decreases with the amount of insulation in the wall and the curves show a greater slope for the higher temperature reservoirs. Lastly, tanks with operating temperatures close to 850K (storage) will have a greater temperature drop than tanks with operating temperatures of 550K (waiting) and also the increase in methanol temperature is less than the decreases that occur in high temperature tanks.

In that regard, it is important to be concerned about maintaining the storage tanks with the lowest level of loss at a higher cost in mineral wool. In brief, the heat leak loss is not important when operating in short cycles of a few hours or days; howefver, it is vital to maintain a good insulation thickness in the tanks to optimize the system in those situations of long waiting and storage periods. It will be seen below that even though the tanks are well insulated, the temperature of the molten salts decreases with time affecting the performance of the PHES technology.

Regarding the influence of climatic conditions (shown in

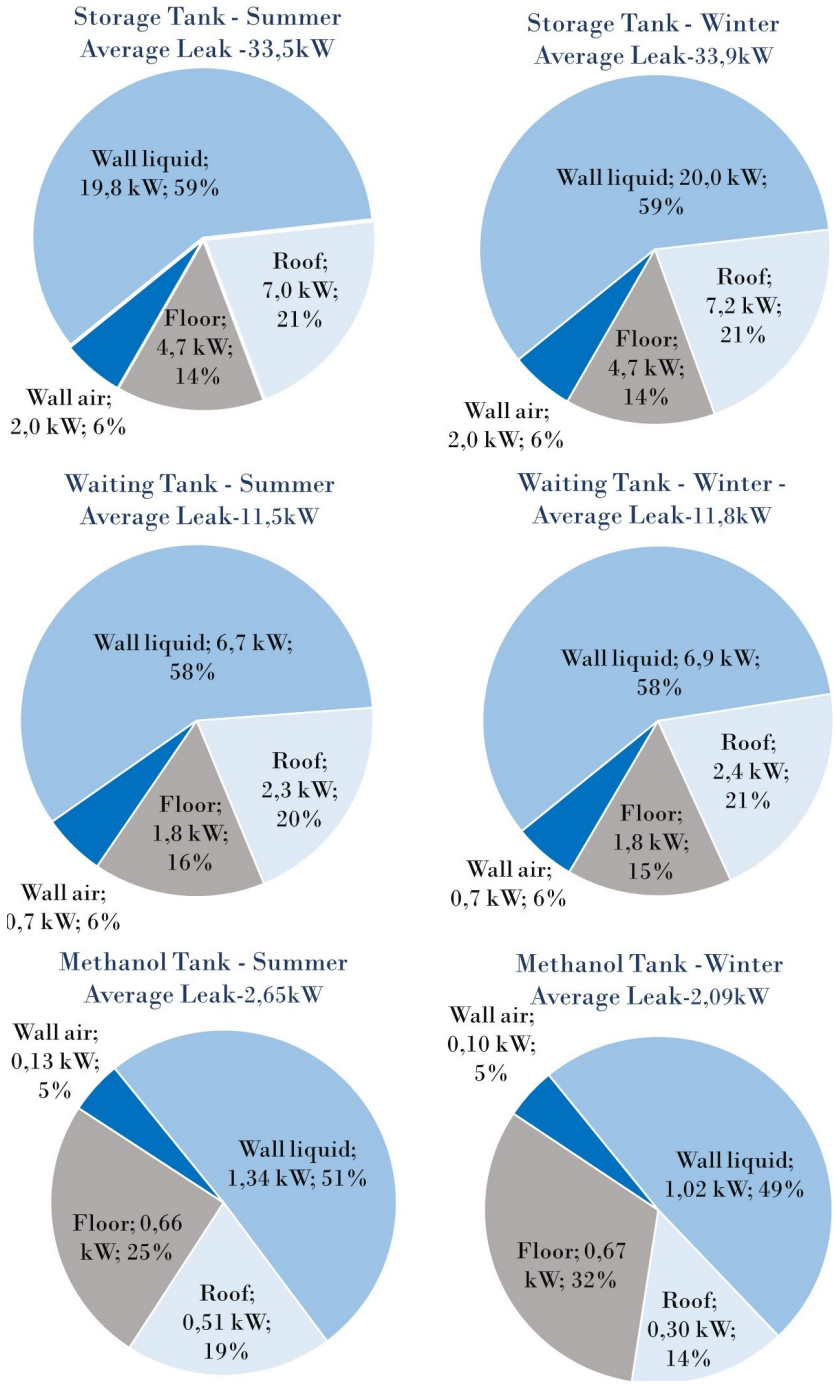

Figure 7: Heat loss fractions for fully charged storage, waiting and methanol tank for average month to summer and winter. Insulation thickness=0.6m (hot temperature) and 0.4m (cold temperature)

Fig. 9) it can be seen that the differences are minimal in high temperature tanks (a.Storage and b.Waiting), but when approaching the surrounding temperature, as in the case of methanol (c.Methanol), such difference starts to become higher. Also, the solar irradiation to the tanks is not very noticeable and only causes lower effects on the heat loss rates, without affecting the global behavior, since the radiation incident to the tank walls does not pass through the insulation and its effect is compensated by the increase in the external wall temperature, which, on the other hand, favors the opposite mechanisms of convection and radiation.

The loss as a function of the filling level for the system charging and discharging periods, which are usually thought for a few hours, can be seen in Fig. 10. In this work, a time of 5 hours is considered.

It is shown that the losses are negligible concerning those occurring during waiting and storage of several days. It is interesting to note the linearly increasing dependence of the heat

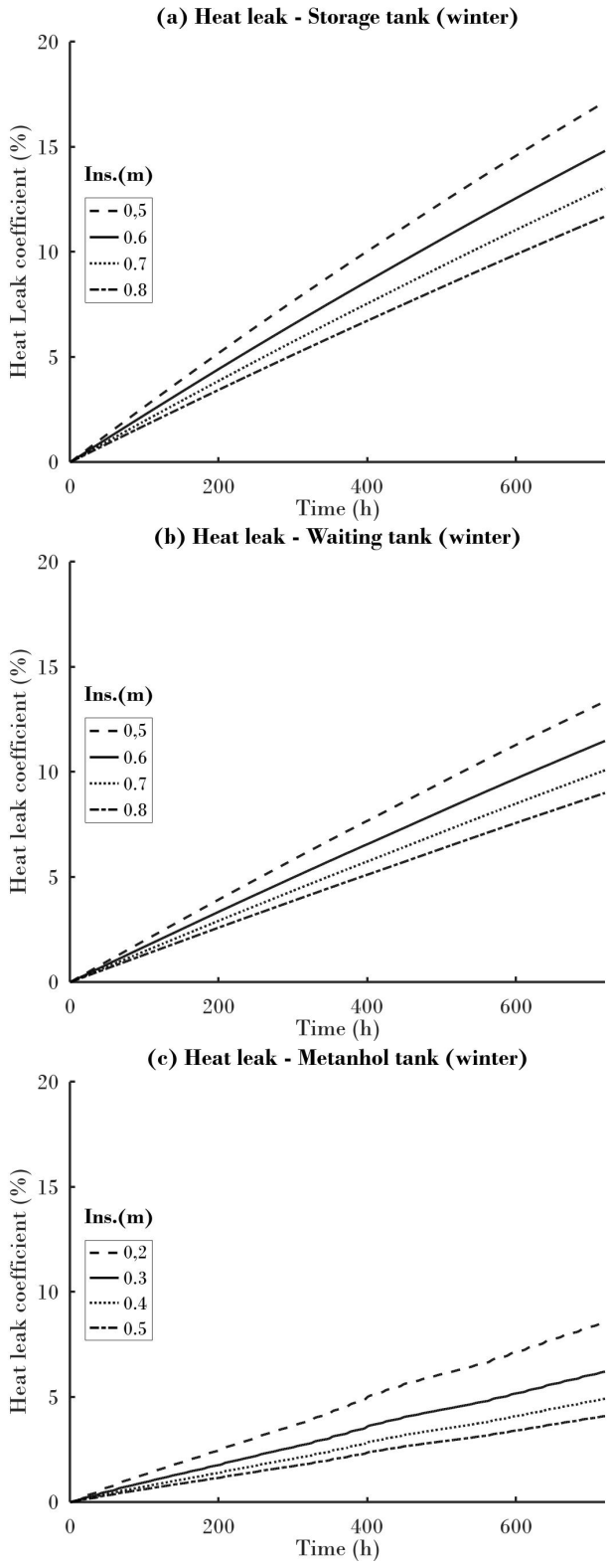

Figure 8: Heat leak variation with time for storage, waiting and methanol tank for different insulation thickness in winter (a) Storage tank (b) Waiting tank (c) Methanol tank.

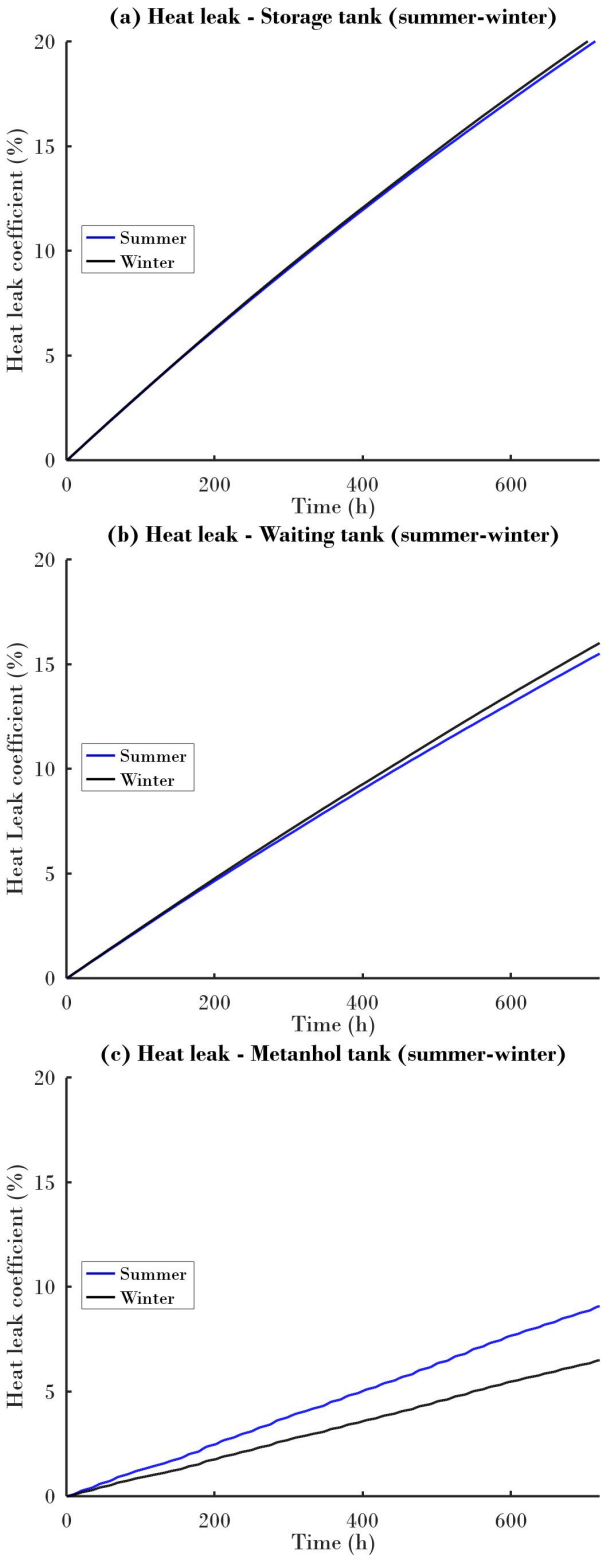

Figure 9: Heat leak vs. time for summer and winter (a) Storage Tank (b) Waiting tank (c) Methanol tank. Insulation thickness=0.6m (hot temperature) and 0.4m (cold temperature).

leak coefficient with increasing level z. However, the cumulative over 5 hours will not have this behavior since the level is variable while the tanks are being emptied or filled.

For long time periods, (See Fig. 11), the temperature decreases within the molten salt volume inside the storage tank (a) and the waiting tank (b), in addition to the increase the tem-

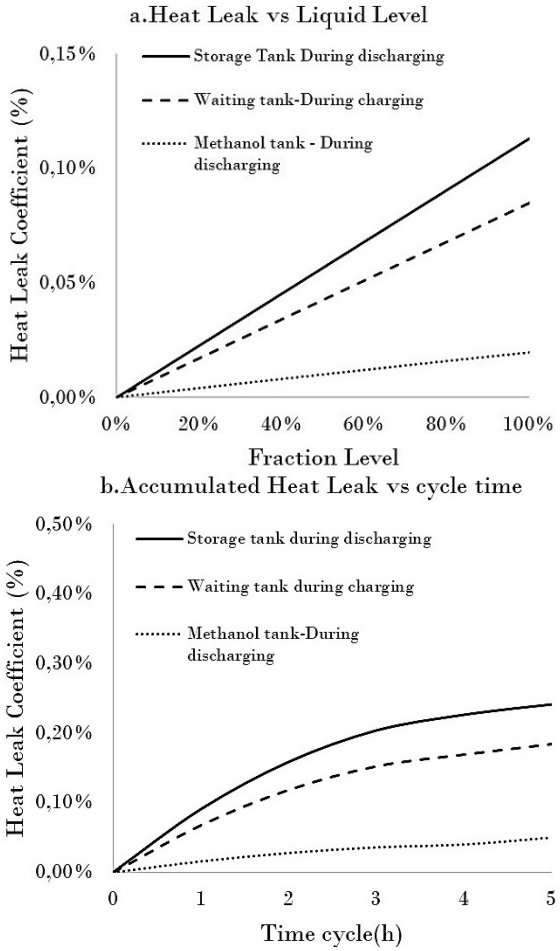

Figure 10: (a) Heat leak coefficient vs. Fraction Level (b) Accumulate heat leak coefficient vs. time cycle (discharging or charging) for storage, waiting and Methanol tank.

perature of the methanol tank (c). A preponderant factor in the design of proposed storage PHES is to avoid crystallization of the thermal liquid. The melting point of commercial solar salt occurs at 511K. The time required for crystallization in each salt reservoir for different insulation thicknesses can be seen on the abscissa axis of Fig. 11. In that regard, the temperature of the storage tank (a) is conditioned by a reduction of the RTE, but not by crystallization. With an appropriate insulation, several months can pass without the need for external heating of the salts to fluidize them. However, the waiting tank (b) is more limited and crystallization periods are closer to one month. Another detail that can be seen in the graphs is that for short periods the temperature curves can approach a linear behavior. When longer analysis times are taken, the trend changes. As shown for methanol (c) no evaporation is expected since the outside temperatures do not reach 337K corresponding to its boiling point, so external influence will in no case limit the use of this cold fluid by a phase change.

As an example, Fig. 12 shows the instantaneous temperatures of the solar salt at the different points of the full storage and waiting tanks after standby in a critical winter month. The behavior is that presented in Fig. 4b. Internally, the profile is quite

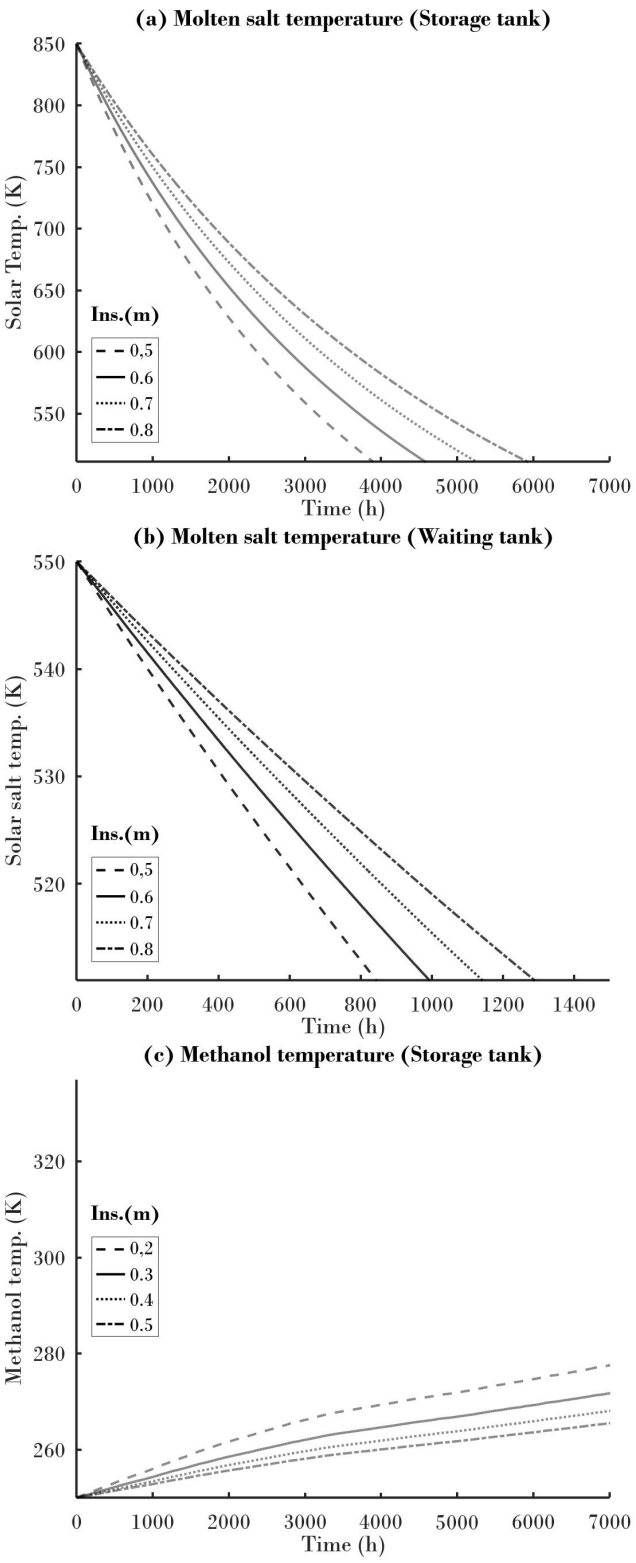

Figure 11: Temperature drop for different insulation thickness (a) Storage Tank and (b) Waiting tank until the crystallization point of the molten salt (511K) (c) Methanol tank until vaporization point (337K).

uniform.

In this work, heat transfer mechanisms conduction, convection and radiation were considered. The order of magnitude of

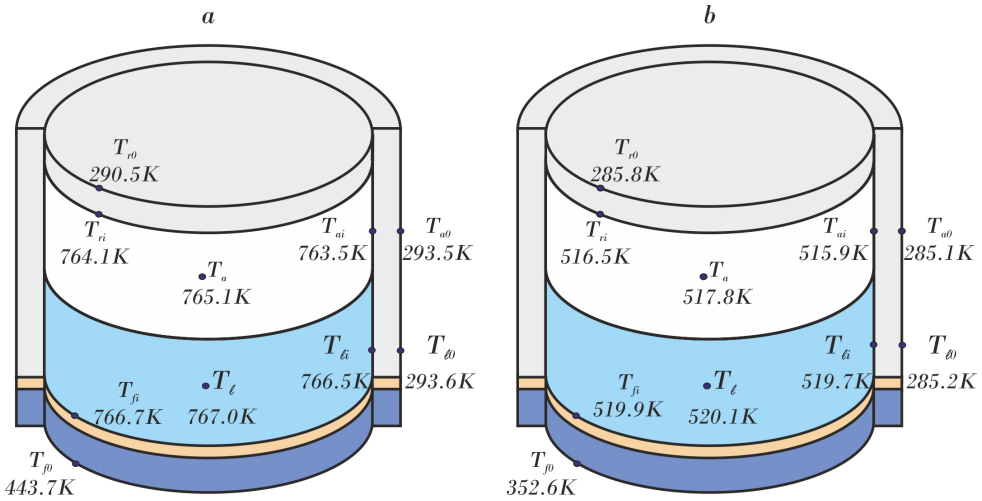

Figure 12: Temperatures in different points of the storage and waiting after 1 month.

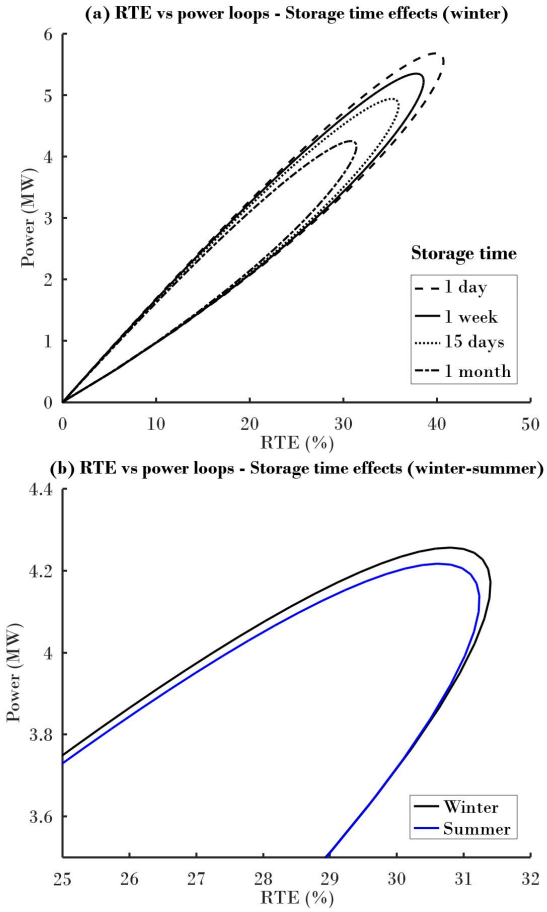

Figure 13: (a) RTE vs. power loops for different storage times (with 15 days of waiting) (b) RTE vs. power loops for winter and summer for 1 month of storage and 15 days of waiting.

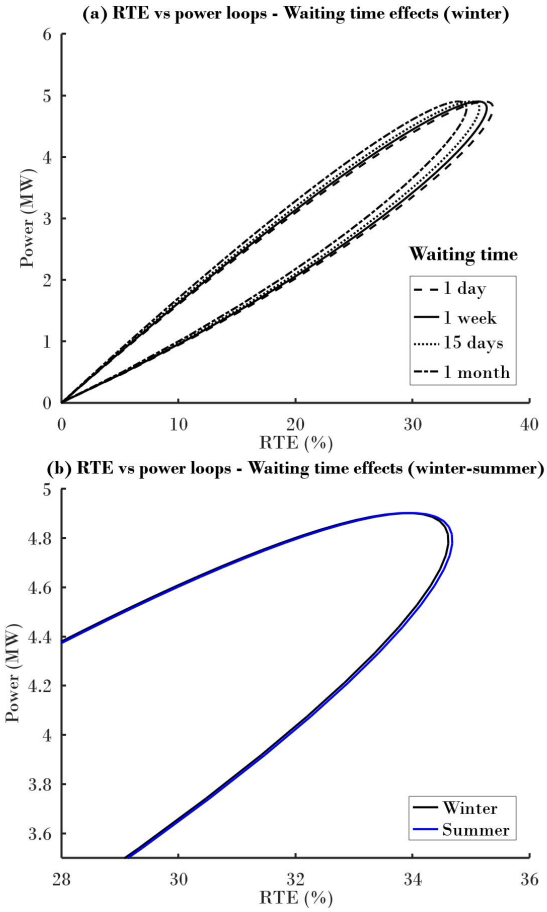

Figure 14: (a) RTE vs. power loops for different waiting times (with 15 days of storage) (b) RTE vs. power loops for winter and summer for 1 month of waiting and 15 days of storage.

the values differs considerably as a function of the insulation thickness, especially for higher levels of the tanks. When the amount of insulating material is large, the conductive thermal resistance of the walls dominates over convection and radiation, the uncertainties of e.g. the Nusselt correlations and the assumed values for emissivities and absorptivities hardly influence the overall heat loss and it can see, for example in Fig. 12, similar temperatures in all the internal tank volume.

In finite time thermodynamics, a tool to represent and analyze the results, commonly used, is the representation of power-

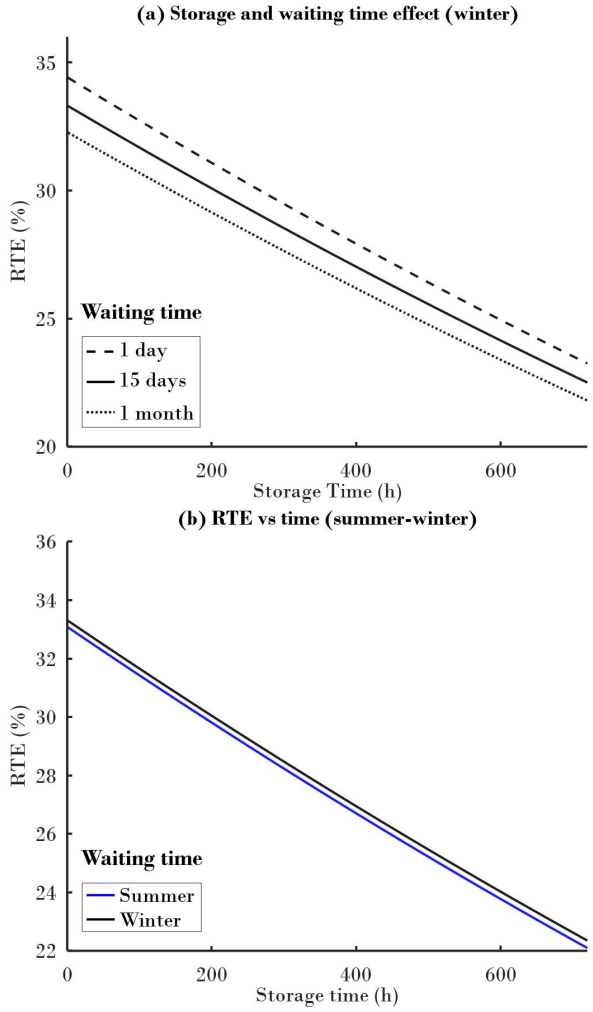

Figure 15: Effect of storage time in RTE (a) For different waiting time in winter (b) For winter and summer. Waiting time=15 days. The insulation is 0.6m for hot storage and 0.4m for cold storage.

performance diagrams. When the power and the round trip efficiency have maximums at different points, by varying a parameter (e.g. pressure ratio), the curve in power-performance diagram shows a loop, and it is easily to visualize both maximums [2]. In Fig. 13 and Fig. 14 this behavior is represented using the pressure ratio (r^{HP}) as a variable, for different storage and waiting periods and also evaluating them for winter and summer periods.

It is noted in Fig. 13, as expected, that the RTE for the proposed case is substantially reduced with the storage time (for one day, one week, 15 days and one month). On the other hand, for the waiting time the effect of the heat leak is much less and you just have to be careful not to reach the crystallization point of the salts (see Fig. 14).

The decrease in RTE performance with storage time is clearly noted for different waiting times in the graph in Fig. 15 where it is also confirmed that for a reduced period there is a practically linear trend of such reduction with time

It can be seen in Fig. 16 how the internal irreversibilities (α) are determinant in the RTE and the incidence of the exchanger efficiency, taken as external irreversibility (β), turns out to be quite lower. As the heat leak effect happens mostly during the storage and waiting periods, the differences in the compression, expansion and heat exchange processes do not have a major influence on the temporal loss and the shown curves are practically parallel to each other.

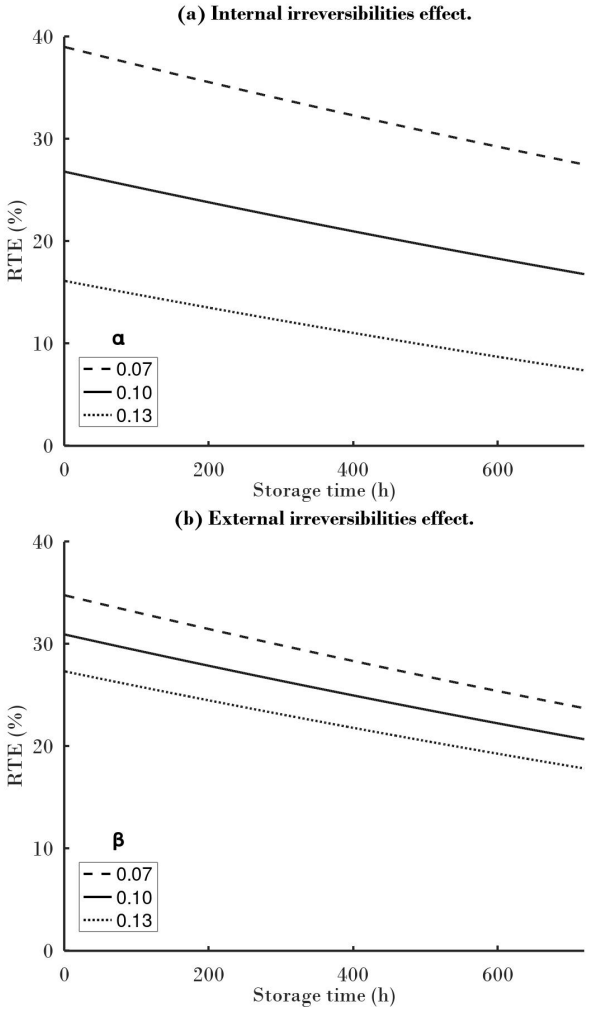

Figure 16: Effect of storage time in RTE (a) For different internal irreversibilities (b) For different external irreversibilities.

In every case, the differences between summer and winter are hardly appreciable, even negligible, since the only noticeable effect is the increase in methanol temperature in summer.

For the analysis of the influence of size plant on heat losses, simulations were performed for 5, 15 and 25 MW with fixed insulation of 0.6m for the salt tanks and 0.4m for the methanol tank. When heat leak, power and RTE are evaluated for different plant sizes in Fig. 17, it is noted how the loss results lower with increasing plant power, benefiting the technology with a lower drop in the energy that can be recovered from the system and the higher RTE. This trend is due to the improvement in the ratio of the mass contained in the reservoir to the transfer area exposed to the environment.

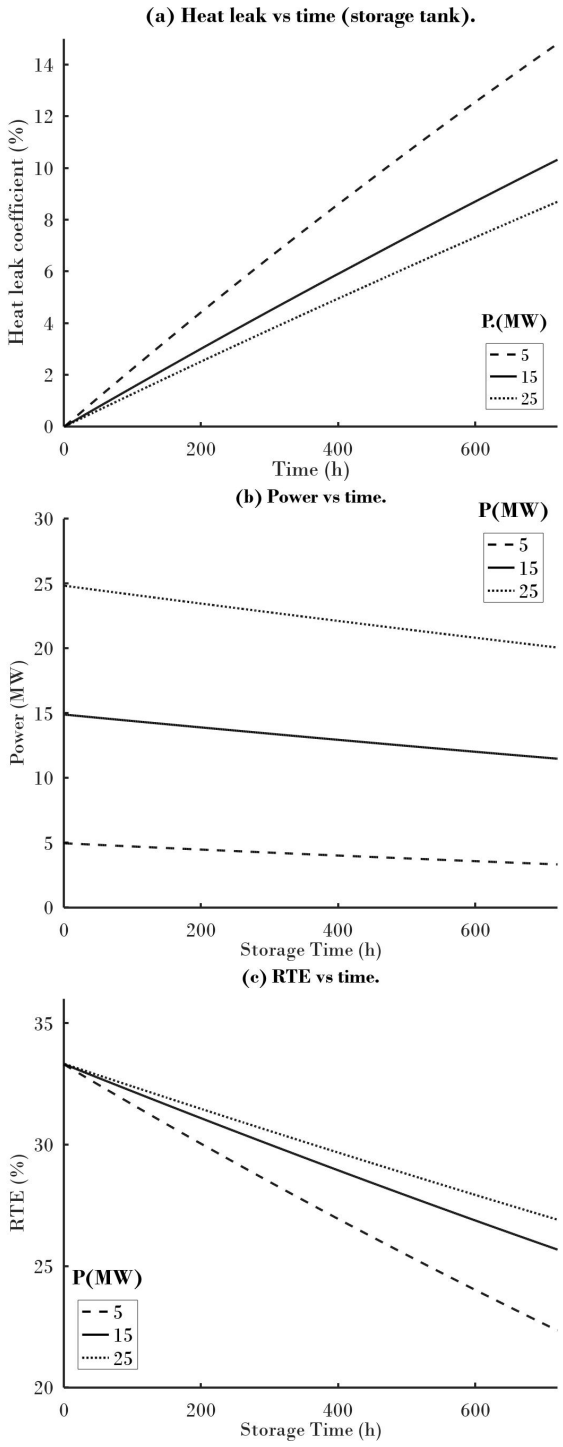

Figure 17: Effect of storage time on (a) heat leak (b) power generation and (c) RTE for different power levels in winter. Insulation thickness=0.6m (hot temperature) and 0.4m (cold temperature).

4. Discussion and conclusions

Sensible thermal storage reservoirs are a very important part of PHES technology. The most studied system for application with thermal fluids is the one that uses nitrate salts as storage medium and hydrocarbons or alcohols, such as methanol, as cold fluid. Molten salts have shown much reliability as storage systems for solar plants and, in that regard, have been selected in this article as a validated way of energy storage.

The present work shows a practical and replicable modeling for any location or required size of PHES plant and allows estimating in a simple way the performance of a technology that may well replace the already known hydraulic storage plants, air reservoirs or chemical batteries due to its relative lower cost, its versatility to be applied in any area and its long useful life.

The novelty of this article, beyond presenting the great potential of the technology itself, is that the proposed model gives the possibility to analyze the round trip efficiency taking the components and the four tanks as a whole, being able to configure various parameters such as cold and storage media, the irreversibilities of the compressors, expanders and heat exchangers, the pressure losses, the working fluids, the insulators, the geometry and properties of the reservoir materials, the size of the plant and even the climatic conditions.

The simulations show that, for this operation mode, there is no risk of salt crystallization during waiting periods of about one month.

Roughly speaking, the effect of the heat leak coefficient in the considered particular case for a 5 MW plant, which reached values of about 20% for the storage tanks, 15% for the waiting tanks and 10% for the methanol tank after one month, affects the RTE by about 0.4% per day for an average thickness of about 10% of the diameter, so that working with greater thicknesses can be interesting when it comes to improving the performance of the technology. The results are favored when the size of the PHES storage plant is increased.

Without considering the returns of the Brayton cycle the results obtained from the simulations, show that storage with solar salts and methanol can become a prosperous technology that will allow stability in the energy demand of the communities even for long reserves periods of liquids in their respective reservoirs.

Acknowledgments

Authors acknowledge financial support from Agencia Nacional de Investigación e Innovación (ANII); Fondo Sectorial de Energía, Uruguay; contract FSE-1-2018-1-153077.

References

[1] A. Benato and A. Stoppato, "Pumped Thermal Electricity Storage: A technology overview," *Thermal Science and Engineering Progress*, vol. 6, pp. 301–315, 2018.

[2] D. Salomone-Gonzalez, J. Gonzalez-Ayala, A. Medina, J. M. Roco, P. L. Curto-Risso, and A. Calvo Hernandez, "Pumped heat energy storage with liquid media: Thermodynamic assessment by a Brayton-like model," *Energy Conversion and Management*, vol. 226, no. August, p. 113540, 2020.

[3] P. Farres-Antunez, H. Xue, and A. J. White, "Thermodynamic analysis and optimisation of a combined liquid air and pumped thermal energy storage cycle," *Journal of Energy Storage*, vol. 18, no. April, pp. 90–102, 2018.

[4] R. B. Laughlin, "Pumped thermal grid storage with heat exchange," *Journal of Renewable and Sustainable Energy*, vol. 9, no. 4, pp. 1–16, 2017.

[5] J. D. McTigue, A. J. White, and C. N. Markides, "Parametric studies and optimisation of pumped thermal electricity storage," *Applied Energy*, vol. 137, pp. 800–811, 2015.
[6] J. Gonzalez, D. Salomone Gonzalez, A. Medina Dominguez, J. Roco, P. L. Curto-Risso, and A. Calvo Hernandez, "Multicriteria optimization of Brayton-like pumped thermal electricity storage with liquid media," *Journal of Energy Storage*,vol. 44, p. 103242, 2021.
[7] F. Zaversky, J. García-Barberena, M. Sánchez, and D. Astrain, "Transient molten salt two-tank thermal storage modeling for CSP performance simulations," *Solar Energy*, vol. 93, pp. 294–311, 2013.
[8] A. K. Araújo and G. I. Medina T., "Analysis of the effects of climatic conditions, loading level and operating temperature on the heat losses of two-tank thermal storage systems in CSP," *Solar Energy*, vol. 176, no. September, pp. 358–369, 2018.
[9] T. Desrues, J. Ruer, P. Marty, and J. F. Fourmigué, "A thermal energy storage process for large scale electric applications," *Applied Thermal Engineering*, vol. 30, no. 5, pp. 425–432, 2010.
[10] J. Guo, L. Cai, J. Chen, and Y. Zhou, "Performance evaluation and parametric choice criteria of a Brayton pumped thermal electricity storage system," *Energy*, vol. 113, pp. 693–701, 2016.
[11] J. Howes, "Concept and development of a pumped heat electricity storage device," *Proceedings of the IEEE*, vol. 100, no. 2, pp. 493–503, 2012.
[12] C. S. Turchi, J. Vidal, and M. Bauer, "Molten salt power towers operating at 600–650C: Salt selection and cost benefits," *Solar Energy*, vol. 164, no. March, pp. 38–46, 2018.
[13] R. Ferri, A. Cammi, and D. Mazzei, "Molten salt mixture properties in RELAP5 code for thermodynamic solar applications," *International Journal of Thermal Sciences*, vol. 47, no. 12, pp. 1676–1687, 2008.
[14] Z. Wan, J. Wei, M. A. Qaisrani, J. Fang, and N. Tu, "Evaluation on thermal and mechanical performance of the hot tank in the two-tank molten salt heat storage system," *Applied Thermal Engineering*, vol. 167, no. December 2019, p. 114775, 2020.
[15] L. Sparks, "Thermal conductivity of a polyurethane foam from 95K to 340K," Tech. Rep. March, 1982.
[16] L. Periglaciares, "Diseño de sistemas de intercambio geotérmico de circuito cerrado," tech. rep., 2017.
[17] N. Pfleger, T. Bauer, C. Martin, M. Eck, and A. Wörner, "Thermal energy storage - overview and specific insight into nitrate salts for sensible and latent heat storage," *Beilstein Journal of Nanotechnology*, vol. 6, no. 1, pp. 1487–1497, 2015.
[18] M. Morandin, F. Maréchal, M. Mercangöz, and F. Buchter, "Conceptual design of a thermo-electrical energy storage system based on heat integration of thermodynamic cycles - Part A: Methodology and base case," *Energy*, vol. 45, no. 1, pp. 375–385, 2012.
[19] J. W. Eaton, *GNU Octave Manual.* Network Theory Limited, 2002.
[20] S. Sanchez, A. Medina and A. Calvo Hernandez, *Thermodynamic model and optimization of a multistep irreversible Brayton cycle,* Energy Conversion and Management, vol. 51, no. 11, pp. 2134–2143, 2010.
[21] J. D. McTigue, C. N. Markides, and A. J. White, "Performance response of packed-bed thermal storage to cycle duration perturbations," *Journal of Energy Storage*, vol. 19, no. September, pp. 379–392, 2018.
[22] C. Suárez, A. Iranzo, F. J. Pino, and J. Guerra, "Transient analysis of the cooling process of molten salt thermal storage tanks due to standby heat loss," *Applied Energy*, vol. 142, pp. 56–65, 2015.
[23] Z. Liu, J. Yan, P. Gao, and H. Tan, "Experimental study on temperature distribution in an ice-making machine multichannel evaporator," *Science and Technology for the Built Environment*, vol. 25, no. 1, pp. 69–82, 2019.
[24] Y. W. Lu, Q. Yu, W. B. Du, Y. T. Wu, and C. F. Ma, "Natural convection heat transfer of molten salt in a single energy storage tank," *Science China Technological Sciences*, vol. 59, no. 8, pp. 1244–1251, 2016.
[25] O. Levenspiel, *Engineering flow and heat exchange*, vol. 6. 3th editio ed., 1985.
[26] Y. Cengel, *Heat Transfer. A practical approach*. 2thedition ed., 2006.
[27] G. Abal, "Fundamentos de Energía Solar - Radiación Solar.," pp. 1–88, 2014.
[28] T. Bergman and A. Lavine, *Fundamentals of heat and mass transfer*. 2017.
[29] A. H. Slocum, W. M. May, T. Supervisor, E. Baglietto, T. Supervisor, G. Chen, T. Reader, and J. Li, *Thermal Fluid characterization and performance enhancement*.
[30] R. Alonso-Suárez, M. Bidegain, G. Abal and P. Modernell, *Año meteorológico típico para aplicaciones de energía solar*, Biblioteca plural, 2019.